Praseodymium 3*d*- and 4*d*-core photoemission spectra of Pr_2O_3

H. Ogasawara
Department of Physics, Faculty of Science, Tohoku University, Sendai 980, Japan

A. Kotani
Institute for Solid State Physics, University of Tokyo, 7-22-1 Roppongi, Minato-ku Tokyo 106, Japan

R. Potze and G. A. Sawatzky
Materials Science Center, University of Groningen, Nijenborgh 18, 9747 AG Groningen, The Netherlands

B. T. Thole
Department of Chemical Physics, University of Groningen, Nijenborgh 16, 9747 AG Groningen, The Netherlands
(Received 2 May 1991)

Experimental data and theoretical calculations are shown for Pr 3*d* and 4*d* x-ray photoemission spectra (XPS) of Pr_2O_3. The observed spectral structures are well explained by the theoretical results that are obtained with the impurity Anderson model by combining intra-atomic multiplet coupling with solid-state hybridization between the Pr 4*f* and O 2*p* states. For 3*d* XPS the main spectral structures are caused by the hybridization effect, while for 4*d* XPS the interplay between the multiplet coupling and the hybridization is essential.

I. INTRODUCTION

Praseodymium ions in Pr_2O_3 are trivalent with a $4f^2$ configuration in the ground state, but in the finale state of Pr 3*d* x-ray photoemission spectra (XPS), the $4f^2$ and $4f^3\,\underline{v}$ ($\underline{v}$ being a hole in the oxygen 2*p* valence band) configurations are strongly mixed through the covalency hybridization, which is induced by a core hole potential acting on the 4*f* electrons. Recently, Ikeda and coworkers[1,2] carried out a systematic analysis of experimental 3*d* XPS spectra[3–5] for various rare-earth sesqui oxides, with the impurity Anderson model, and showed the importance of the final-state hybridization effect for Pr_2O_3, as well as for La_2O_3 and Ce_2O_3. They disregarded the effect of intra-atomic multiplet coupling, which is considered to be less important than the effect of the hybridization for 3*d* XPS. For 4*d* XPS of Pr_2O_3, on the other hand, the multiplet coupling is expected to be very important, because the exchange interaction between 4*d* and 4*f* states is much larger than that between 3*d* and 4*f* states. It is the purpose of the present paper to study, both experimentally and theoretically, the interplay between the intra-atomic multiplet coupling and the solid-state hybridization in the 4*d* XPS (and also 3*d* XPS) of Pr_2O_3.

Experimentally, the 4*d* XPS of the Pr_2O_3 were measured by Burroughs *et al.*[4] about 15 years ago. However, the accuracy of the data is not sufficient for detailed study of the multiplet structures. Therefore, we performed more precise measurements of 4*d* XPS, as well as 3*d* XPS, with a good quality Pr_2O_3 sample. For the theoretical analysis, we recently developed a method of calculating x-ray absorption and photoemission spectra, taking account of both the multiplet effect and the hybridization, by combining Cowan's atomic-multiplet program[6] with the impurity Anderson model calculation. We have applied our technique to the analysis of 3*d* and 4*d* x-ray-absorption spectra[7,8] in CeO_2 and PrO_2; this is an application to the analysis of XPS of rare-earth systems. As shown later on, the 4*d* XPS of the free Pr^{3+} ion exhibits very complicated multiplet terms which are extended over an energy range of about 30 eV. Our method has made it possible to combine such complicated multiplet terms with the solid-state hybridization in the impurity Anderson model, extending the recent analysis[9] of 4*d* XPS for less complicated systems La_2O_3 and Ce_2O_3 to systems with $4d^9 4f^3\underline{v}$ final states. Thus, the 4*d* XPS of Pr_2O_3 is not only an interesting object in the study of the interplay between multiplet coupling and hybridization but also one of the most appropriate systems in testing our new calculation method.

In Sec. II experimental procedures and the observed data of Pr 3*d* and 4*d* XPS are given, and in Sec. III these data are analyzed theoretically. Section IV is devoted to some discussion.

II. EXPERIMENT

A pressed pellet of black Pr_6O_{11} was reduced under flowing hydrogen at 850 °C for 20 h and subsequently quenched to room temperature.[10] The so obtained pale green pellet was identified with x-ray diffraction as the hexagonal single phase with cell constants $a = 3.86$ Å and $c = 6.02$ Å.[11] In this phase the Pr ion is surrounded by seven oxygen ions: four at a short and three at a somewhat longer distance. (There also exists a cubic phase in which the Pr ion is surrounded by six oxygen ions in a strongly distorted octahedron, and this phase occurs

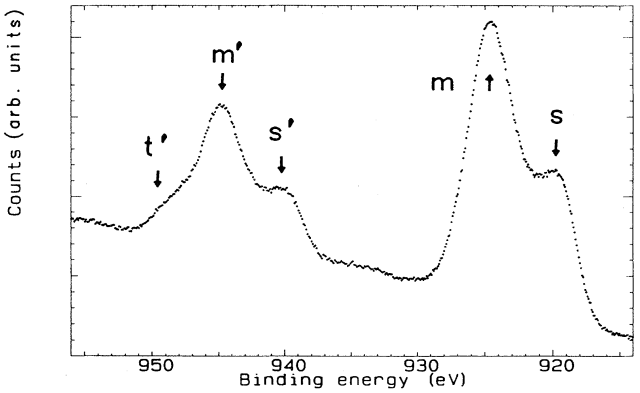

FIG. 1. Experimental result of Pr $3d$ XPS for Pr_2O_3. The spectra consist of $3d_{3/2}$ and $3d_{5/2}$ components with higher and lower binding energies, respectively. The arrows m and m' indicate main peaks, s and s' satellites, and t' indicates an extra structure which exists only in the $3d_{3/2}$ component.

when we reduce to temperatures below 700 °C.)

The pellet was attached to a sample holder and measured with a commercially available X-Probe 300 from Surface Science Instruments. The x-ray source is the monochromated Al $K\alpha$ (1486.6 eV) line. The spectra were recorded at a pressure of $<10^{-9}$ Torr with a spot size of 600 μm. Pr_2O_3 is a large-band-gap insulator. Due to charging effects peak broadening and peak shifts occurred. By heating the sample to 300 °C and using a floodgun with low-energy electrons the broadening due to charging was minimized. Because of remaining charging and the influence of the floodgun the absolute binding energies are accurate to only a few eV. By scraping the sample with a diamond file in ultrahigh vacuum the shoulder on the oxygen $1s$ peak due to surface hydroxide formation could be strongly reduced.

The experimental results for $3d$ and $4d$ XPS of Pr_2O_3 are shown in Figs. 1 and 2, respectively. These data are

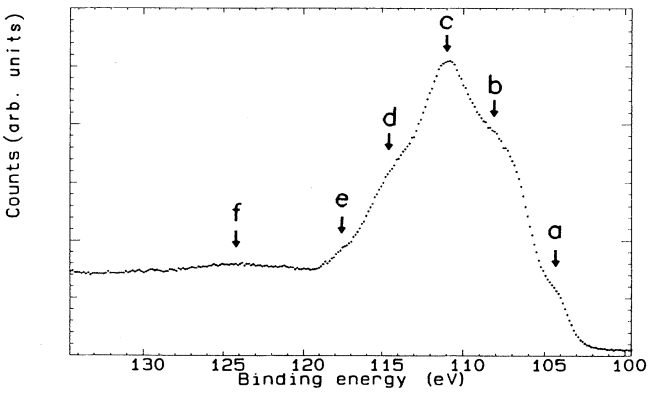

FIG. 2. Experimental result of Pr $4d$ XPS for Pr_2O_3. The spectra cannot be divided into $4d_{3/2}$ and $4d_{5/2}$ components because they overlap each other. The arrows a, b, d, and e indicate shoulders, c the highest peak, and f indicates a broad bump.

similar to those observed by Burroughs *et al.*,[4] but some spectral structures are found more clearly with better resolution. The observed $3d$ XPS shows the main peaks m and m', and the satellites s and s' for $3d_{5/2}$ and $3d_{3/2}$ components, respectively. In the $4d$ XPS, we recognize spectral shoulders a, b, d, and e, and also a broad bump f, which will be compared in detail with the theoretical results in the next section.

III. THEORY

The Hamiltonian consists of the two parts,

$$H=H_1+H_2\ , \tag{1}$$

where H_1 is the Hamiltonian of the usual impurity Anderson model,

$$\begin{aligned} H_1=&\sum_{k,\nu}\varepsilon_k a^\dagger_{k\nu}a_{k\nu}+\varepsilon_f\sum_{\nu}a^\dagger_{f\nu}a_{f\nu}+\varepsilon_d\sum_{\xi}a^\dagger_{d\xi}a_{d\xi}\\ &+\frac{V}{\sqrt{N}}\sum_{k,\nu}(a^\dagger_{f\nu}a_{k\nu}+a^\dagger_{k\nu}a_{f\nu})\\ &+U_{ff}\sum_{\nu>\nu'}a^\dagger_{f\nu}a_{f\nu}a^\dagger_{f\nu'}a_{f\nu'}\\ &-U_{fc}\sum_{\nu,\xi}a^\dagger_{f\nu}a_{f\nu}(1-a^\dagger_{d\xi}a_{d\xi})\ , \end{aligned} \tag{2}$$

and H_2 describes the atomic Coulomb, exchange, and spin-orbit interactions, as given in Ref. 7. The energies ε_k, ε_f, and ε_d represent the O $2p$ valence band, the Pr $4f$ level, and the Pr $3d$ (or $4d$) level, respectively. We assume that ε_k is given by N discrete levels in the form

$$\varepsilon_k=\varepsilon_v-\frac{W}{2}+\frac{W}{N}(k-\tfrac{1}{2}),\quad k=1,\ldots,N \tag{3}$$

where ε_v and W are, respectively, the center and the width of the valence band. The index ν represents the spin and orbital magnetic quantum numbers of the f state, and ξ those of the $3d$ (or $4d$) state. The interactions V, U_{ff}, and $-U_{fc}$, respectively, are the hybridization between $4f$ and valence-band states, the Coulomb interaction between $4f$ electrons, and the core hole potential acting on the $4f$ electron.

The parameter values in the impurity Anderson model are taken to be the same as those estimated by a previous analysis (without multiplet coupling) of $3d$ XPS by Ikeda *et al.*:[1] $\Delta=10.5$ eV, $V=0.56$ eV, and $U_{fc}(3d)=13.0$ eV, where the charge-transfer energy Δ is defined by $\Delta\equiv\varepsilon_f-\varepsilon_v+2U_{ff}$. The value U_{fc} for the $4d$ core state is taken to be 80% of $U_{fc}(3d)$. Some discussion on this reduction factor will be given in Sec. IV. The main effects of valence band ε_k are obtained with a single level ($N=1$), but the effect of its finite width will also be studied with $N=3$ and $W=2.5$ eV. Slater integrals and spin-orbit coupling constants included in H_2 are calculated by an atomic Hartree-Fock program with relativistic corrections,[8] and then the Slater integrals $F^k(4f4f)$, $F^k(3d4f)$, $G^k(3d4f)$, $F^k(4d4f)$, and $G^k(4d4f)$ are reduced by 20%, 20%, 20%, 25%, and 33%, respectively. The values of the reduced Slater integrals and the spin-

TABLE I. Slater integrals and spin-orbit parameters (all values in eV).

nd	$F^2_{(4f,4f)}$	$F^4_{(4f,4f)}$	$F^6_{(4f,4f)}$	ζ_{4f}	ζ_{nd}	$F^2_{(nd,4f)}$	$F^4_{(nd,4f)}$	$G^1_{(nd,4f)}$	$G^3_{(nd,4f)}$	$G^5_{(nd,4f)}$
$3d$	11.0	7.0	5.0	0.13	8.1	6.9	3.2	4.8	2.8	1.9
$4d$	11.0	7.0	5.0	0.13	1.4	11.2	7.2	11.7	7.3	5.2

orbit coupling constants are listed in Table I. The Hamiltonian matrix elements both for the ground state and the final state and the optical transition matrix elements between these states are obtained using Cowan's program.[6] The Hamiltonian matrices are diagonalized numerically within the subspace of $4f^2$ and $4f^3\underline{v}$ configurations ($d^9 4f^2$ and $d^9 4f^3\underline{v}$ configurations for the final state), where $\underline{v}$ is a state of f symmetry, and between the eigenstates the XPS spectra are calculated.

The calculated $3d$ and $4d$ XPS are shown in Figs. 3 and 4, respectively. Here we use $N=1$, and the origin of the binding energy is taken arbitrarily. The continuous spectra are obtained by convoluting the line spectra with a Lorentzian function with the width Γ(HWHM)$=0.7$ eV where HWHM is the half-width at half maximum. The results are in satisfactory agreement with the experimental data. When we compare Fig. 3 with Fig. 1(c) of Ref. 1 where the multiplet effect was neglected, we find that the main spectral structures are almost unchanged; the satellite s (or s') is mainly caused by the effect of the covalency hybridization, and the multiplet effect gives some modification of the spectral shape and broadening. One of the important roles of the multiplet effect is to cause a difference in the spectral shape between $3d_{5/2}$ and $3d_{3/2}$ components. As shown in Fig. 1, the observed $3d_{3/2}$ spectrum exhibits an intensity rise t' on the higher-energy tail of the main line, which is absent for the $3d_{5/2}$ spectrum. This feature is well reproduced in our calculation (Fig. 3). However, the calculated spectrum includes some additional structures near t' and r in Fig. 3 that are not observed in Fig. 1.

The calculated $4d$ XPS (Fig. 4) exhibits the spectral features $a \sim f$, which nicely correspond to those observed in Fig. 2. In order to see the effects of the multiplet coupling and the solid-state hybridization separately, we calculate $4d$ XPS by changing the value V. The results for $V=0$, 0.2, 0.4, and 0.8 eV are shown in Figs. 5(a), 5(b), 5(c), and 5(d), respectively. Figure 5(a) corresponds to the $4d$ XPS of free Pr^{3+} ion, which has wide spread multiplet structures due to the strong Coulomb and exchange interactions. This spectrum is very different from the experimental one for Pr_2O_3. From Figs. 4 and 5(b)–5(d), it is clearly seen that the effect of V strongly changes the atomic multiplet structure of Fig. 5(a). The experimental result (Fig. 2) is reproduced well only for the value $V \sim 0.56$ eV (Fig. 4). Therefore, we conclude that the interplay between the atomic multiplet coupling and the solid-state hybridization is essential in forming the $4d$ XPS spectrum.

The agreement between the theoretical and experimental results is further improved by taking account of the finite width of the O $2p$ valence band. The results of $3d$

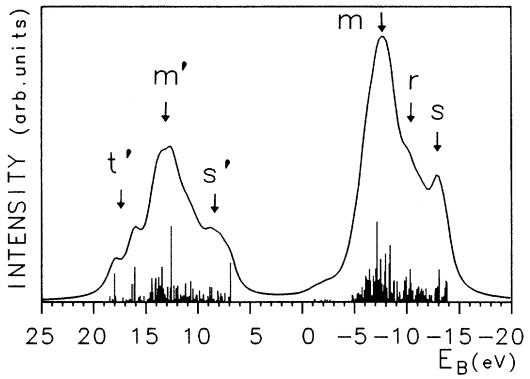

FIG. 3. Theoretical result for $3d$ XPS. The line spectra are convoluted with a Lorentzian function with Γ(HWHM)$=0.7$ eV. The arrows m and m' indicate main peaks, s and s' satellites, and t' indicates an extra structure which is caused by the multiplet effect. The arrow r indicates an additional shoulder which cannot be seen in the experimental result. The solid-state parameters used are $N=1$, $\Delta=10.5$ eV, $U_{fc}=13.0$ eV, $V=0.56$ eV. The Slater integrals and the spin-orbit parameters are given in Table I.

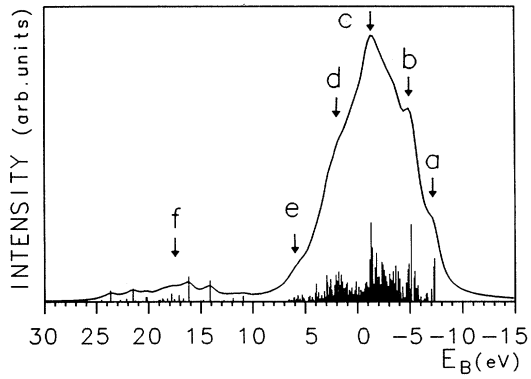

FIG. 4. Theoretical result for $4d$ XPS. The line spectra are convoluted with a Lorentzian function with Γ(HWHM)$=0.7$ eV. The arrows a, b, d, and e indicate shoulders, c the highest peak, and f indicates broad structures due to large exchange splittings. The solid-state parameters used are $N=1$, $\Delta=10.5$ eV, $U_{fc}=10.5$ eV, $V=0.56$ eV. The Slater integrals and the spin-orbit parameters are given in Table I.

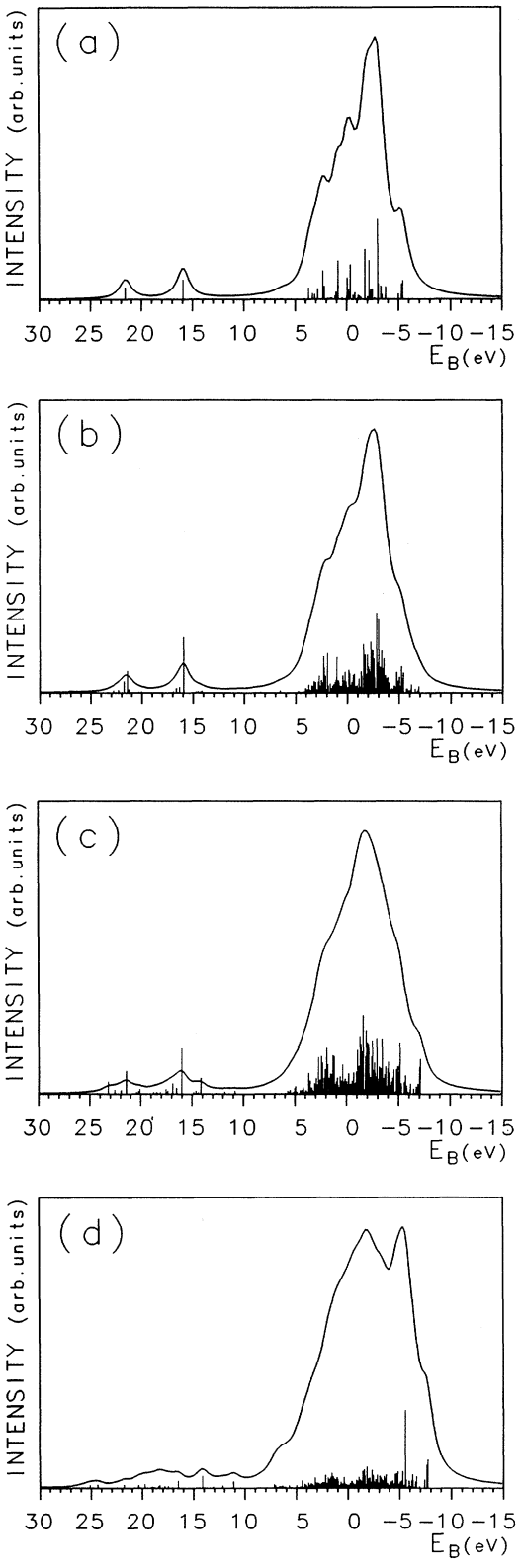

FIG. 5. Theoretical results for 4*d* XPS with different hybridization strength. The other parameters are the same as those in Fig. 4. (a) is the result for $V=0$ eV, which corresponds to the spectrum of the free Pr^{3+} ion. In (b), (c), and (d), the values of V are 0.2, 0.4, and 0.8 eV, respectively.

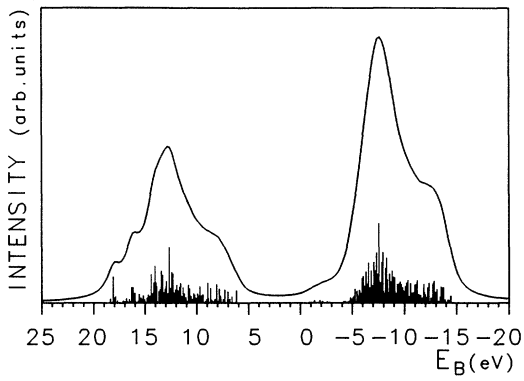

FIG. 6. Theoretical result for 3*d* XPS with finite width of the O 2*p* valence band. The number of levels in the valence band is $N=3$, and the bandwidth is $W=2.5$ eV. The other parameters are the same as those in Fig. 3.

and 4*d* XPS calculated with $N=3$ and $W=2.5$ eV are shown in Figs. 6 and 7, respectively. The effect of the finite band width is to smear out some structures which occurred in Figs. 3 and 4. For instance, the structure *r* in Fig. 3 is smeared out in Fig. 6, and the kink *b* and some fine structures near *f* in Fig. 4 are rounded in Fig. 7, in better agreement with experimental results.

IV. DISCUSSION

In the ground state of Pr_2O_3, the Pr ion is almost trivalent with $4f^2$ configuration. The convalancy mixing between the $4f^2$ and $4f^3\underline{v}$ configurations is quite small, because the charge transfer energy Δ ($=10.5$ eV) is much larger than the hybridization V ($=0.56$ eV). In the final state of XPS, on the other hand, the charge transfer energy decreases down to $\Delta_f \equiv \Delta - U_{fc}$ due to the existence of the core hole potential, so that Δ_f becomes comparable with V. For 3*d* XPS, the value of Δ_f is estimated to be

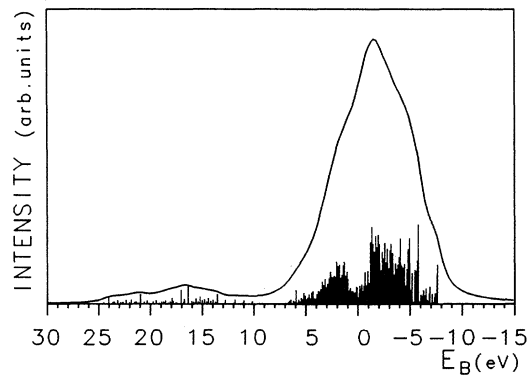

FIG. 7. Theoretical result for 4*d* XPS with a finite width of the O 2*p* valence band. The number of levels in the valence band is $N=3$, and the bandwidth is $W=2.5$ eV. The other parameters are the same as those in Fig. 4.

-2.5 eV, and we have a strong covalency mixing; the final states contributing to the main peak of $3d$ XPS are, on the average, a 0.76:0.24 mixture of $4f^2$ and $4f^3\underline{v}$ configurations, while those of the satellite are a 0.24:0.76 mixture.

In the case of $4d$ XPS, the core hole potential $-U_{fc}(4d)$ is weaker than $-U_{fc}(3d)$. According to the Hartree-Fock calculation, the ratio $U_{fc}(4d)/U_{fc}(3d)$ is about 0.8. In our calculation we have changed $U_{fc}(4d)$ as an adjustable parameter around 0.8 $U_{fc}(3d)$, but actually the calculated $4d$ XPS agrees best with the experiment for $U_{fc}(4d)=0.8U_{fc}(3d)=10.5$ eV. With this value of $U_{fc}(4d)$, we obtain $\Delta_f \equiv \Delta - U_{fc}(4d)=0$. This means that the covalency mixing in the final state of $4d$ XPS is extremely strong; the mixing rate between $4f^2$ and $4f^3\underline{v}$ should be about 0.5:0.5. In order to see the effect of the strong covalency mixing on $4d$ XPS, we remove from Fig. 4 the multiplet effect except the $4d$ spin-orbit coupling. Then the $4d$ XPS reduces, as shown in Fig. 8, to four discrete lines: the m and s lines associated with the $4d_{5/2}$ core level and their $4d_{3/2}$ partners m' and s'. Figures 5(a) and 8 correspond to two limiting situations, where the intra-atomic multiplet coupling and the solid-state hybridization, respectively, play a dominant role in the $4d$ XPS. However, both of them fail in explaining the spectral features $a \sim f$ of the observed $4d$ XPS, which are reproduced only in an intermediate situation (Fig. 4) between the two extremes.

In conclusion, the $4d$ XPS of Pr_2O_3 originates from the interplay between the strong intra-atomic multiplet coupling and the strong solid-state hybridization. We believe that the successful calculation of the spectral features $a \sim f$ in Pr $4d$ XPS shows that the impurity model is not only capable of reproducing charge transfer satellite energy positions and intensities but also the detailed changes in the multiplet structure. There is still no apparent need for refinements of the model. Our new technique of calculating XPS multiplet structures in covalent systems, using more group theory, is capable of treating more complicated f shell configurations than before and has already been applied successfully to the XPS spectra of transition-metal compounds.[12–14]

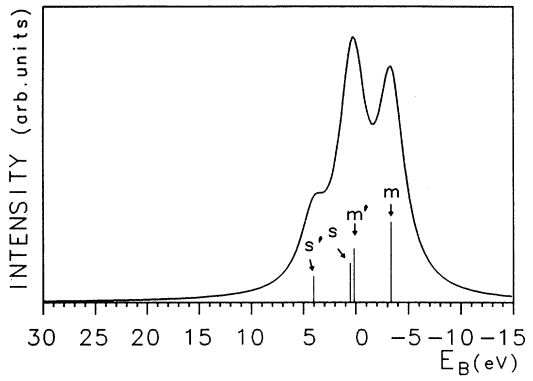

FIG. 8. Theoretical result for $4d$ XPS without the multiplet effect. The lines m and s indicate the main line and the satellite, and m' and s' are their spin-orbit partners.

ACKNOWLEDGMENTS

The authors would like to thank Dr. K. Okada for discussion. A part of this work was carried out while one of the authors (A.K.) stayed at the University of Groningen. This work was partially supported by the International Joint Research Project from the Japan Society for the promotion of Science (JSPS) and a Grant-in-Aid for Scientific Research from the Ministry of Education, Science and Culture in Japan.

[1]T. Ikeda, K. Okada, H. Ogasawara, and A. Kotani, J. Phys. Soc. Jpn. **59**, 622 (1990).
[2]A. Kotani, T. Ikeda, K. Okada, and H. Ogasawara, J. Electron Sectrosc. Relat. Phenom. **51**, 229 (1990).
[3]J. C. Fuggle, M. Campagna, Z. Zotnierek, R. Lässer, and A. Platru, Phys. Rev. Lett. **45**, 1597 (1980).
[4]P. Burroughs, A. Hamnett, A. F. Orchard, and G. Thornton, J. Chem. Soc. Dalton Trans. **17**, 1686 (1976).
[5]M. Aono, S. Kawai, S. Kono, M. Okusawa, T. Sagawa, and Y. Takehara, Solid State Commun. **16**, 13 (1974).
[6]R. Cowan, *The Theory of Atomic Structure and Spectra* (University of California Press, Berkeley, 1981).
[7]A. Kotani, H. Ogasawara, K. Okada, B. T. Thole, and G. A. Sawatzky, Phys. Rev. B **40**, 65 (1989).
[8]H. Ogasawara, A. Kotani, K. Okada, and B. T. Thole, Phys. Rev. B **43**, 854 (1991).
[9]S. Imada and T. Jo, J. Phys. Soc. Jpn. **58**, 402 (1989); **58**, 2665 (1989).
[10]J. S. Anderson and K. J. Gallagher, J. Chem. Soc. 52 (1963).
[11]H. R. Hockstra, Inorg. Chem. **5**, 754 (1966).
[12]K. Okada, A. Kotani, B. T. Thole, and G. A. Sawatzky, Solid State Commun. **76**, 1277 (1990).
[13]K. Okada, A. Kotani, B. T. Thole, and G. A. Sawatzky, Solid State Commun. **77**, 835 (1991).
[14]K. Okada and A. Kotani, J. Phys. Soc. Jpn. **60**, 772 (1991).